APPLIED AND ENVIRONMENTAL MICROBIOLOGY, May 2005, p. 2501–2510 Vol. 71, No. 5
0099-2240/05/$08.00+0 doi:10.1128/AEM.71.5.2501–2510.2005

Application of a pH-Sensitive Fluoroprobe (C-SNARF-4) for pH Microenvironment Analysis in *Pseudomonas aeruginosa* Biofilms

Ryan C. Hunter* and Terry J. Beveridge

Department of Microbiology, University of Guelph, Guelph, Ontario N1G 2W1, Canada

Received 24 September 2004/Accepted 26 November 2004

An important feature of microbial biofilms is the development of four-dimensional physical and chemical gradients in space and time. There is need for novel approaches to probe these so-called microenvironments to determine their effect on biofilm-specific processes. In this study, we describe the use of seminaphthorhodafluor-4F 5-(and-6) carboxylic acid (C-SNARF-4) for pH microenvironment analysis in *Pseudomonas aeruginosa* biofilms. C-SNARF-4 is a fluorescent ratiometric probe that allows pH quantification independent of probe concentration and/or laser intensity. By confocal scanning laser microscopy, C-SNARF-4 revealed pH heterogeneity throughout the biofilm in both the *x*,*y* and *x*,*z* planes, with values ranging from pH 5.6 (within the biofilm) to pH 7.0 (bulk fluid). pH values were typically remarkably different than those just a few micrometers away. Although this probe has been successfully used in a number of eukaryotic systems, problems have been reported which describe spectral emission changes as a result of macromolecular interactions with the fluorophore. To assess how the biofilm environment may influence fluorescent properties of the dye, fluorescence of C-SNARF-4 was quantified via spectrofluorometry while the probe was suspended in various concentrations of representative biofilm matrix components (i.e., proteins, polysaccharides, and bacterial cells) and growth medium. Surprisingly, our data demonstrate that few changes in emission spectra occur as a result of matrix interactions below pH 7. These studies suggest that C-SNARF-4 can be used as a reliable indicator of pH microenvironments, which may help elucidate their influence on the medical and geobiological roles of natural biofilms.

In natural environments, microbes preferentially live in matrix-enclosed, complex, integrated communities known as biofilms. The fully mature biofilm is typified by a three-dimensional structure made up of bacterial cells, a microbe-derived polymer matrix, and interstitial water channels that facilitate the exchange of nutrients and wastes with the surrounding environment. A most remarkable feature of these complex biofilm communities is the development of chemical gradients (i.e., pH, redox potential, and ions) due to the differential diffusion of nutrients, metabolic products, and oxygen throughout the biofilm (1, 14, 49, 50, 54). These gradients are partitioned into so-called microenvironments produced by the diverse microbial physiology and local physicochemical properties found within a biofilm, so that the conditions within a microenvironment can be profoundly different from those encountered in the bulk phase.

This feature of biofilms has been recognized in a number of natural and clinical environments. For example, the heterogeneous charge distribution of various matrix polymers is thought to contribute to biofilm antimicrobial tolerance through sorption or deactivation of chemically reactive biocides (20, 24, 25, 31, 35). pH and redox gradients within biofilms have also been implicated in driving global geochemical cycles by altering the speciation of inorganic ions (9, 27, 30, 32). Although the concept of the microenvironment is widely accepted, its dynamic spatial and temporal complexity makes it difficult to define precise associations between these gradients and specific biofilm processes. Accordingly, there is a need for novel approaches to define the physical and chemical properties of biofilm microenvironments. Such approaches will help elucidate the environmental and clinical phenomena driven by small aggregates of cells within microbial communities.

Gradients of ion concentrations have been extensively studied in the past, either at the micrometer scale by means of microelectrodes (1, 6, 15, 37, 39, 41, 51, 54, 56) or at higher resolution using fluorescent imaging in which probes exhibit spectral emission changes in response to changing ion concentrations (12, 50). These techniques, however, are not without their limitations—microelectrode resolution is restricted (i.e., based on electrode tip size), ion-sensitive probes are not always suitable for quantitative microscopy (due to compartmentalization and photobleaching of the probe) (2, 50), and highly advanced technologies (such as multiphoton microscopy) (40, 45) are not accessible to all laboratories. Ratiometric imaging has been recently introduced (47); here, protonation of specific fluorophores shifts their emission spectra so that increasing ion concentration increases fluorescent intensity at one wavelength and decreases it at another. The ratio of intensities obtained at both wavelengths serves as a quantitative measure of pH. This method has previously been applied to biofilm systems (4, 16) but not with the probes used in our report; the older probes used previously have been discontinued. 5-(and-6)-Carboxyseminaphthorhodafluor-1 (C-SNARF-1) is a ratiometric dye that has seen considerable use in studying $[H^+]$ in eukaryotic systems (2, 3, 33, 34, 52). To our knowledge, however, its use in microbial systems has not been reported.

This study assesses the potential of a fluorinated derivative of C-SNARF-1, seminaphthorhodafluor-4F 5-(and-6)-carboxylic acid (C-SNARF-4), as a quantitative indicator of pH mi-

* Corresponding author. Mailing address: Department of Microbiology, CBS, University of Guelph, Guelph, Ontario N1G 2W1, Canada. Phone: (519) 824-4120, ext. 58904. Fax: (519) 837-8702. E-mail: rhunte01@uoguelph.ca.

croenvironments in microbial biofilms. C-SNARF-4 has dual-emission properties but has a slightly lower pH sensitivity maximum (pK_a ~6.4) relative to its other C-SNARF relatives, making it more suitable for use in the slightly acidic environments expected in our biofilms (21). We have used C-SNARF-4 in combination with confocal scanning laser microscopy (CSLM) to study single-species *Pseudomonas aeruginosa* communities and the pH of their microenvironments. Since there have been recent reports suggesting C-SNARF emission characteristics can be influenced by the probe's interaction with various cell components (7, 23, 38, 48, 55), we wanted to determine the extent to which biofilm components (i.e., proteins, exopolymers, and bacterial cells) influence C-SNARF-4 emission properties. Accordingly, spectrofluorometric analyses were used to determine the effect of representative matrix components (alginate, bovine serum albumin, *P. aeruginosa* cells, and growth medium) on the spectral emission properties of the fluorophore. Novel fluorescent techniques such as this are required to fully understand the contributions of pH microenvironments to biofilm-specific processes.

MATERIALS AND METHODS

Bacterial strains, culture conditions, and biofilm development. *Pseudomonas aeruginosa* PAO1 was used throughout this study and was obtained from J. Lam (University of Guelph). To visualize biofilm growth, a *gfp*-tagged PAO1 was used possessing plasmid pMF230 (36), which contained the gene for green fluorescent protein (GFP) containing the *mut2* mutation (13). GFP was expressed constitutively. Strains were maintained on Trypticase soy agar (Becton Dickinson). When required, carbenicillin was added at 300 μg per ml. A dilute broth medium (Trypticase soy broth [TSB]) was used for the flow system to grow biofilms at a concentration of 3 g per liter (dTSB), which is 1/10 the recommended concentration. The pH of dTSB was adjusted to 6.8. When bacteria containing pMF230 were analyzed, 50 μg of carbenicillin per ml was added to the dTSB.

Biofilms were cultivated at room temperature in single-channel flow cells (1 by 10 by 40 mm; Biosurface Technologies Inc., Bozeman, MT) supplied with dTSB at a flow rate of 0.1 ml/min for 7 days using a Manostat Carter multichannel peristaltic pump (Barnant, Barrington, IL). Flow cells were sterilized using 75% (vol/vol) ethanol. Once sterile, flow cells were conditioned with dTSB for 24 h, at which point the flow system was inoculated with an overnight culture of PAO1 (optical density at 600 nm = 0.6) through an upstream injection port. After inoculation, flow was arrested to facilitate bacterial adhesion for 1 h. Following attachment, flow was resumed and the substrate was pumped through at a constant rate of 0.1 ml/min for 7 days.

Spectrofluorometric assays. To calibrate C-SNARF-4 photon emissions and to assess the dye's potential use in probing biofilm microenvironments, small volumes of a 1 mM stock solution of C-SNARF-4 in dimethyl sulfoxide were added to pH-adjusted 50 mM HEPES. Final pHs were 5.6, 6.0, 6.4, 6.8, 7.2, and 7.6. The final probe concentration ranged from 1 μM to 10 μM to determine the effects of compartmentalization on emission intensity. Samples were mixed, allowed to equilibrate for 15 min, and transferred to a quartz cuvette (path length, 0.5 cm). C-SNARF-4 emission spectra were recorded on a Quantamaster C-61 steady-state spectrofluorometer (Photon Technology International, Lawrenceville, NJ) using an excitation wavelength of 488 nm, emission wavelengths of 580 nm and 640 nm, and a slit width of 2 nm. To determine the C-SNARF-4 fluorescence ratio, background fluorescence (bkgd) was subtracted at each emission wavelength 640 and 580 nm) as calculated in equation 1.

$$\text{Ratio} = (\text{Em}_{640} - \text{Em}_{640,\text{bkgd}})/(\text{Em}_{580} - \text{Em}_{580,\text{bkgd}}) \quad (1)$$

Titration curves were calculated and used to convert fluorescence emission ratios to pH. To assess the influence of matrix components on C-SNARF-4 emissions, samples were prepared by adding C-SNARF-4 (10 μM) to pH-adjusted dTSB or characteristic matrix components (10^5 cells; 1% or 2% [wt/vol] alginic acid or 1% or 2% [wt/vol] bovine serum albumin [BSA]) in pH-adjusted HEPES. All samples were mixed, allowed to equilibrate for 15 min, and quantified via spectrofluorometry using the calibration sample settings. Emission ratios were determined according to equation 1.

Confocal scanning laser microscopy. All biofilm images were collected using a Leica TCS SP2 CSLM (Leica) equipped with an Ar/Kr 488-nm laser, and a 488/514 dichroic beam splitter which provided optimal signal analysis from the GFP and C-SNARF-4. A 40×/1.00 positive low Fluotar oil immersion lens was used to collect 2,056- by 2,056-bit resolution images in the *x*,*y* and *x*,*z* planes. Depths quoted in this paper are the distances from the substratum to the focal plane.

GFP-tagged biofilms were excited at 488 nm and emission was detected at 510 nm. Since our CSLM does not lend itself to continuous monitoring of biofilm growth, flow cells were clamped to stop dTSB flow and imaged within 15 min. GFP intensity was quantified using LCS confocal software.

To determine the spatial distribution of pH microenvironments, biofilms were treated with 1 ml of dTSB supplemented with C-SNARF-4 at a final concentration of 10 μM. Once biofilms reached maturity (7 days), flow cell inputs were clamped, and spent medium was carefully removed via a syringe through the upstream injection port. The fresh dTSB–C-SNARF-4 solution was carefully introduced through the same injection port to minimize structural damage to the biofilm. Flow cells were clamped, and biofilms were imaged within 15 min of flow stoppage to minimize the accumulation of acidic metabolites, which may artificially modify local pH microenvironments. C-SNARF-4-treated biofilms were excited at 488 nm, and emission was detected in two channels at 580 nm and 640 nm. pH microenvironments were determined from a series of two-channel optical sections by calculating the ratio of emission intensity (i.e., pixel values) between the two channels ($\text{Em}_{640\ \text{nm}}/\text{Em}_{580\ \text{nm}}$). All intensities were determined using LCS software. Images were enhanced using Photoshop software (Adobe, Mountain View, Calif.) for presentation purposes only.

Identical calibration standards were used for CSLM as they were for spectrofluorometry, though only 10 μM C-SNARF-4 was used. Samples were mixed and imaged in 200-μl sample wells and imaged using settings identical to those for the biofilm samples. Titration curves of ratios versus pH were calculated using LCS software according to equation 1 and were used to convert C-SNARF-4 emissions ratios to biofilm pH values. As a control, untreated biofilms were also imaged to ensure that autofluorescence of biological material would not interfere with pH quantification.

Image analysis. C-SNARF-4 emissions within the biofilm were evaluated with LCS software by selecting 20 regions of interest from the image pairs (580 nm and 640 nm). Each region of interest was ~50 μm^2 of biofilm area, providing an average measure of pH within each region. The regions of interest were selected from the bulk fluid phase and microcolony fringes and throughout the centers of microcolonies. Emission ratios between the two image pairs were determined, and pHs were determined based on calibration titration curves.

RESULTS

Fluorescence spectra in buffer. C-SNARF-4 was calibrated in a series of pH-adjusted buffers (pH 5.6 to 7.6, the expected pH levels in the biofilm) at various concentrations. As our data were obtained spectrofluorometrically, as well as by quantitative CSLM imaging, we measured an identical set of calibration solutions by both techniques. The calibrated emission spectra (540 nm to 680 nm) for C-SNARF-4 (10 μM) obtained in pH-adjusted HEPES solutions are shown in Fig. 1a and b. When samples were excited in the fluorometer at 488 nm, the emission spectrum of the probe exhibited peaks of fluorescence emission at 580 nm and ~650 nm (Fig. 1a). As the pH of the solution increased from 5.6 to 7.6, emission intensities recorded at 580 nm decreased, whereas the emission intensities recorded at 640 nm increased. The intensities of the two channels were equal at approximately pH 6.4. When quantified by CSLM, the emission bands also had their maxima close to 580 nm and 640 nm, and intensities at both wavelengths underwent similar changes in response to increasing pH levels (Fig. 1b). However, in this system, emission intensities were significantly greater at the shorter wavelength (580 nm) than the spectrofluorometry data, while they remained relatively consistent at the higher wavelength (640 nm). This suggests

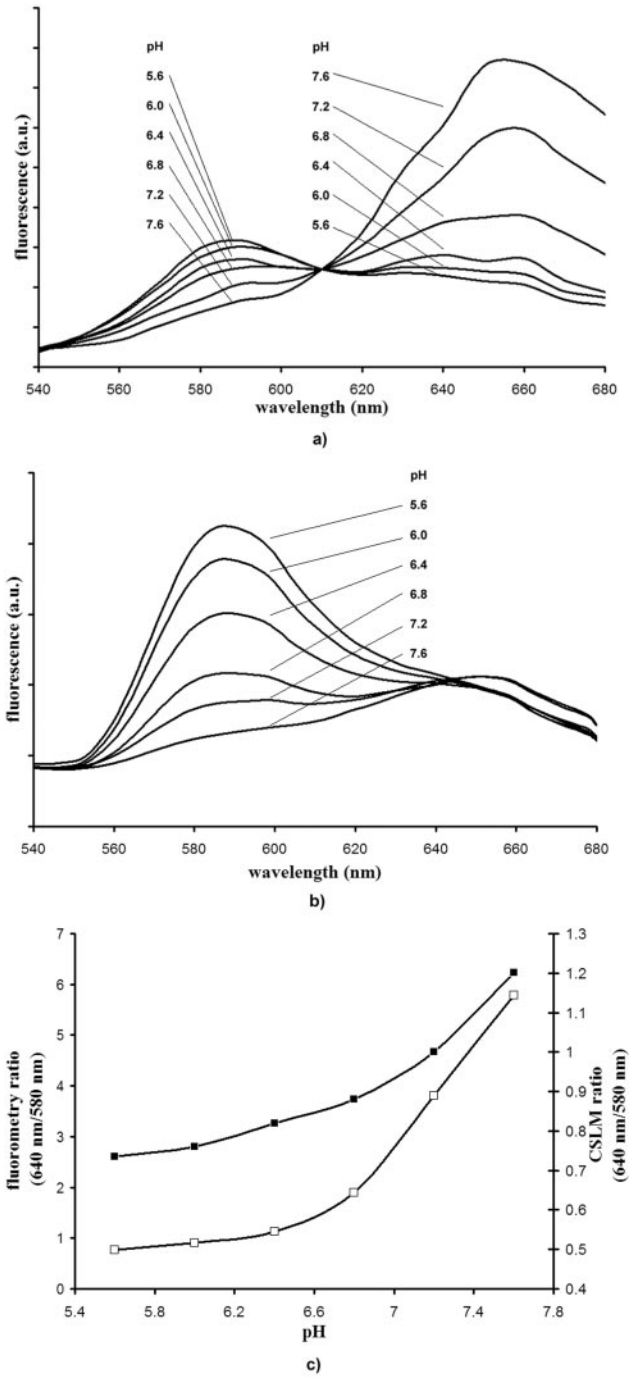

FIG. 1. Emission spectra of C-SNARF-4 in various pH-adjusted HEPES solutions, buffered to pH 5.6, 6.0, 6.4, 6.8, 7.2, and 7.6. Identical samples were excited at 488 nm and fluorescence emission levels (arbitrary units [a.u.]) were recorded by spectrofluorometry (a) or CSLM (b). (c) Corresponding emission intensity ratios (640 nm/580 nm) for spectrofluorometric data (□) and CSLM emissions (■). Note that emission ratios remained constant, although emission spectra varied according to probe concentrations (1 μM, 2 μM, and 10 μM).

that C-SNARF-4 probe fluorescence ratios can be influenced by the spectral sensitivity of the instrument used.

To use these data to determine pH in biofilm systems, the ratio of emission intensities at 640 to 580 nm were determined and shown in Fig. 1c. Standard deviations of fluorometry-derived calibration ratios ranged from ~0.3 pH units at near-neutral pH values (i.e., pH 7.6) to less than 0.1 pH unit at more acidic pH values (pH 5.6). CSLM ratios showed a standard deviation of less than 0.2 pH units at all pH levels used in this experiment. When decreasing fluorophore concentrations were used (1 μM and 5 μM), emission intensities decreased significantly in both systems; however, the emission intensity ratios seen here remained constant for each instrument at all concentrations (data not shown). These observations corroborate that emission ratios are proportional to pH and will not be affected by compartmentalization of the probe throughout the matrix.

CSLM micrographs depicting SNARF fluorescence intensity in 50 mM HEPES adjusted to pH 5.6 and 7.2 are shown in Fig. 2. Image pairs at 580 nm (green) and 640 nm (red) are combined in each micrograph. These two images clearly show a difference in green and red pixel intensity at acidic and neutral pH values, suggesting that SNARF-4 can be used in combination with confocal microscopy to visually identify pH microenvironments that exist within PAO1 biofilms.

SNARF interaction with matrix components. To assess potential interactions of CSNARF-4 with components of the biofilm matrix and the growth medium, the probe was incubated with various concentrations of exopolysaccharides (alginate), protein (BSA), bacterial cells (*P. aeruginosa* PAO1), and growth medium (dTSB). Spectrofluorometric analysis revealed that from pH 5.6 to 7.0, there was little difference in C-SNARF-4 emissions whether in pH-adjusted buffer or in the presence of matrix components (Fig. 3a). Above pH 7.2, however, bacterial cell/C-SNARF-4 samples revealed an increase in fluorescent intensity ratio (640 nm/580 nm), and showed even greater variation at pH 7.6. This was not surprising, though, since some of our images showed internalization of the pH probe by *P. aeruginosa* cells (Fig. 3b), which likely regulated their internal pH at a level more alkaline than that of the surrounding environment. Internalization would lead to protonation-deprotonation of the probe, thus influencing its emission intensity. At pH 7.6, emission ratios were slightly higher in alginic acid and BSA samples, though this variation translated into a difference of only 0.2 pH units. (It is possible that the higher concentration of ionizable carboxylate groups on the alginic acid somehow affected the emission characteristics of C-SNARF-4.) These results suggest that even if the fluorophore does become bound or interacts with biofilm components, particularly alginate and BSA, C-SNARF-4 is still highly sensitive to pH changes and alters its emission spectra accordingly.

When various concentrations of BSA and alginate were used (0.5, 1.0, and 2%), emission ratios below pH 7.0 remained constant, while fluorescence above 7.0 showed a concentration-dependent change in emission intensity (data not shown). This indicated that a heterogeneous distribution of matrix components throughout the biofilm could result in emission ratio variation of C-SNARF-4 in slightly alkaline microenvironments.

Biofilm growth and microbiology. Due to the dynamic nature of a microenvironment, it is important to establish a point in time when the biofilm has matured to a quasi-steady state in terms of its three-dimensional architecture before characteriz-

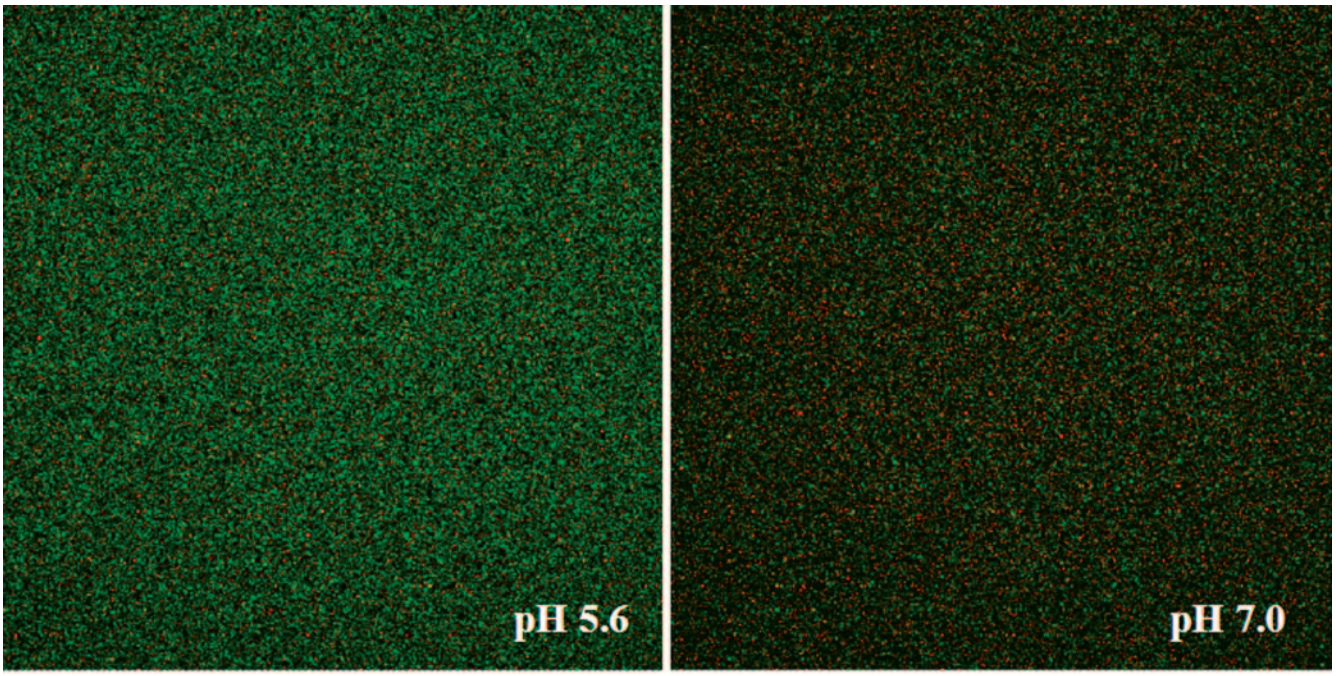

FIG. 2. CSLM image slices of SNARF-4 suspended in pH-adjusted 50 mM HEPES buffer. Samples were imaged in 200-μl sample wells, and fluorescence intensity was independent of depth throughout the sample. The ratio of intensity of the red channel to green (640 nm/580 nm) is indicative of the ambient pH. Although concentration changes can affect pixel intensities, C-SNARF-4 concentrations in these two micrographs are identical (10 μM).

ing the gradients that have developed within it. GFP-labeled PAO1 provided easy monitoring of biofilms over the course of 7 days, by allowing us to visualize cells as they reconfigured their community. Though GFP did not reveal the distribution of extracellular polymers throughout the biofilm, we felt that this probe gave an accurate representation of biofilm structure in CSLM. Early biofilm development (24 to 48 h) frequently revealed individual cells colonizing the flow cell surface, while only a few small clusters of cells were observed (data not shown). Only after 60 h did the microcolonies start to develop

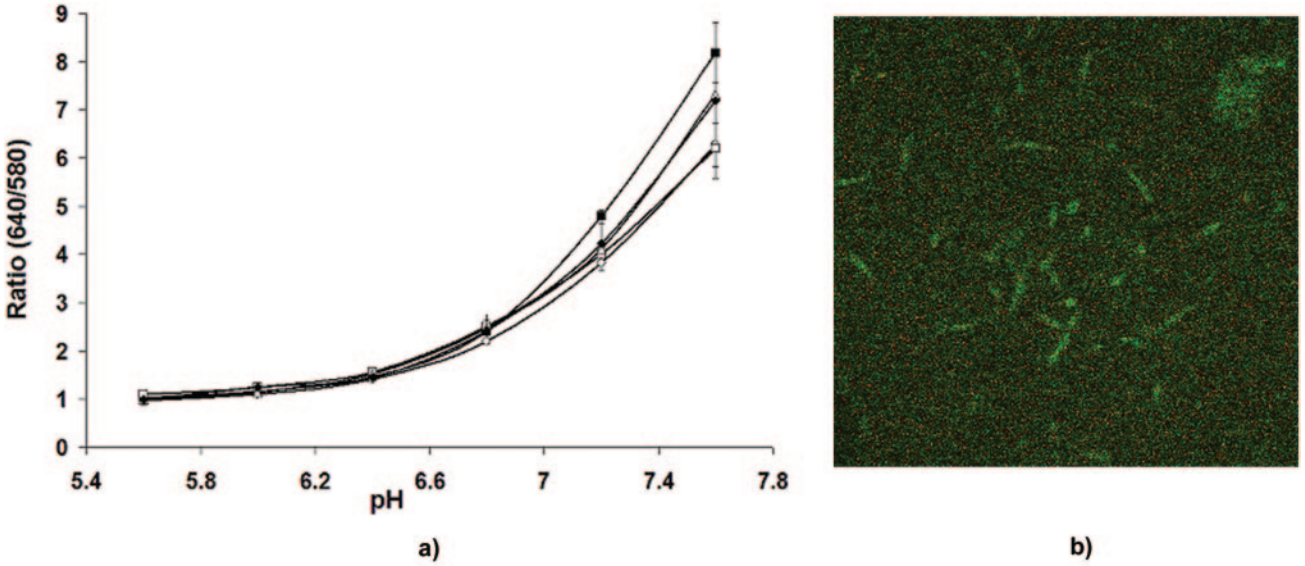

FIG. 3. (a) Fluorescence ratios of C-SNARF-4 from stained suspensions of representative matrix components (Δ, 1% alginic acid; ♦, 1% BSA; ■, 10^5 CFU/ml *P. aeruginosa*; ○, dTSB; □, 50 mM HEPES). Above pH 7, bacterial cells, alginic acid, and BSA showed a concentration-dependent increase in emission ratios, suggesting an interaction of biofilm matrix components with C-SNARF-4. (b) C-SNARF-treated *Pseudomonas aeruginosa* planktonic cells. Some microbes show internalization of the probe, which can alter fluorescence emission levels due to intracellular pH differences.

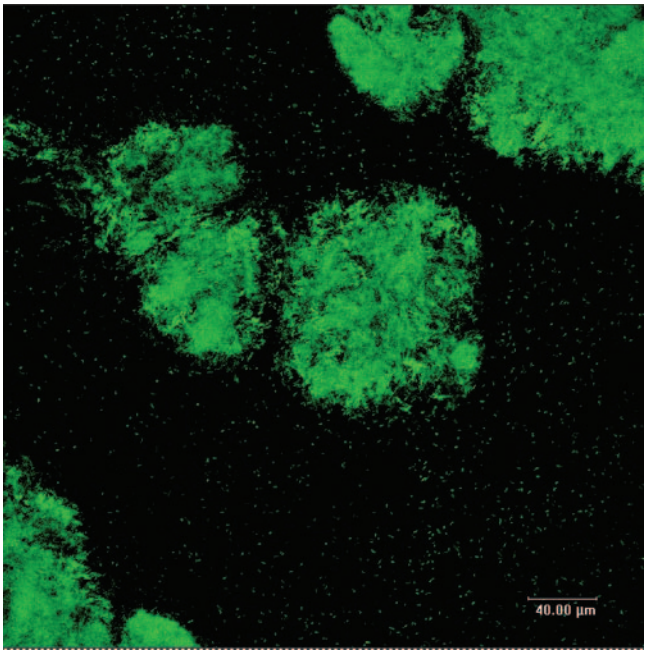

FIG. 4. CSLM micrograph of GFP-labeled PAO1 showing biofilm morphology after 7 days of growth. Subsequent biofilm development maintained an average thickness of ~40 μm and an average diameter of ~90 μm, indicating a pseudo-steady state. Bar, 40 μm.

vertically into structures typical of *P. aeruginosa* biofilms. After 72 h of cultivation, biofilm communities began to show distinct structural features, typified by cell clusters (microcolonies) organized into 80- to 100-μm-diameter pillar structures that were separated by large areas of uncolonized substratum (Fig. 4). As biofilms continued to grow past this point, microcolonies maintained an average thickness of ~40 μm and an average diameter of ~90 μm. Based on the consistency of these structural features (thickness and diameter), it was determined that after 96 h of flow-cell cultivation, biofilms had reached maturity (i.e., quasi-steady state). It was likely that pH microenvironments at this point were most representative of natural conditions in mature biofilms. As a result, it was these biofilms that were subjected to further C-SNARF-4 analysis.

pH microenvironments in PAO1 biofilms. C-SNARF-4 allowed us to visualize acidic microenvironments in *P. aeruginosa* PAO1 biofilms. Figures 5b, c, and d reveal a typical C-SNARF-4-treated biofilm at three different focal planes in *x* and *y* of the microcolony that is shown in the bright-field micrograph in Fig. 5a. The thickness of the microcolony was approximately 50 μm and focal planes are shown at 40-μm (5b), 20-μm (5c), and 5-μm (5d) distances from the substratum. pH values were determined for 5 to 10 regions of interest within three different areas of the biofilm (bulk fluid, microcolony edges, and center of the microcolony). By determining the ratio of pixel intensity (red/green) in these regions, we were able to distinguish the presence of distinct horizontal pH heterogeneity throughout the biofilm. pH imaging at the 40-μm plane (Fig. 5b) revealed a nearly homogenous pH profile, with an average pH of 6.7 ± 0.1. pH values in the bulk fluid and within the microcolony tended to be within 0.2 pH units of the growth medium (pH 6.8). Some areas appeared to have lower fluorescence intensity than the rest of the region within the micrograph, which may indicate restricted diffusion of the probe into the microcolony. However, ratiometric calculations account for a lower concentration of probe within the biofilm. pH profiles obtained closer to the substratum (i.e., deeper in the biofilm) (Fig. 5c and d) showed much more pH variation relative to the microcolony at the fluid-biofilm interface. The pH values shown at 20 μm from the substratum (Fig. 5c) ranged from 6.1 ± 0.3 at the center of the microcolony to 6.3 ± 0.2 at the edges of the biofilm. More alkaline microenvironments tended to be located in areas towards the edge of the biofilm, although this varied depending on sampling location. C-SNARF-4 emissions nearest the substratum (Fig. 5d) also showed remarkable variation in pH relative to higher regions of the biofilm. At this depth, average pH values towards the center of the microcolony (6.0 ± 0.3) were also more acidic than the surrounding areas (6.3 ± 0.2), although this also varied depending on location. In virtually all regions of the biofilm, pH values were often quite different from regions of the same biofilm just a few micrometers away. In all focal planes, bulk fluid pH generally remained near neutral, although a slight drop in pH was observed (0.2 U) in some areas, typically nearest the substratum (not shown). These data suggest a significant heterogeneous environmental chemistry throughout and on the exterior of the biofilm matrix.

A typical *x,z* profile also shows distinct pH variation (Fig. 6). As seen in the horizontal cross-sections, pH values in the center of the microcolony were generally more acidic than those in the bulk fluid phase (~6.8, the pH of the growth medium). Average values near the biofilm-fluid interface were 6.4 ± 0.2, whereas average pH levels deeper in the biofilm were 6.1 ± 0.3. In some areas, however, pH was more alkaline in deeper regions of the biofilm than in surrounding areas, and no identifiable pH gradients (i.e., top to bottom) were seen throughout this study.

The highest pH detected in this study was 7.0, and this was found in the bulk fluid phase, whereas the most acidic environment detected (pH 5.6) was located in the center of a microcolony (values not shown). No detectable levels of fluorescence were present in untreated biofilms, which confirmed that autofluorescence of biological material did not contribute to pH measurements (data not shown).

DISCUSSION

As microbial communities mature, the heterogeneous consumption of nutrients and production of metabolic wastes, in combination with diffusion limitations on chemical species throughout the biofilm matrix, generate so-called microenvironments (i.e., those minute regions associated with biofilms that are a few micrometers in diameter). These become remarkably different from the physical and chemical conditions that exist in the surrounding bulk fluid phase. Although this heterogeneity is well recognized, the direct implications of these microenvironments (notably pH and redox potential) on biofilm-specific phenomena have been elusive and difficult to detect at high spatial resolution in real time. For example, microelectrodes have difficulty monitoring regions <10 to 25 μm^2, and their physical insertion can perturb the biofilm, affecting cell growth and matrix physicochemistry. For this rea-

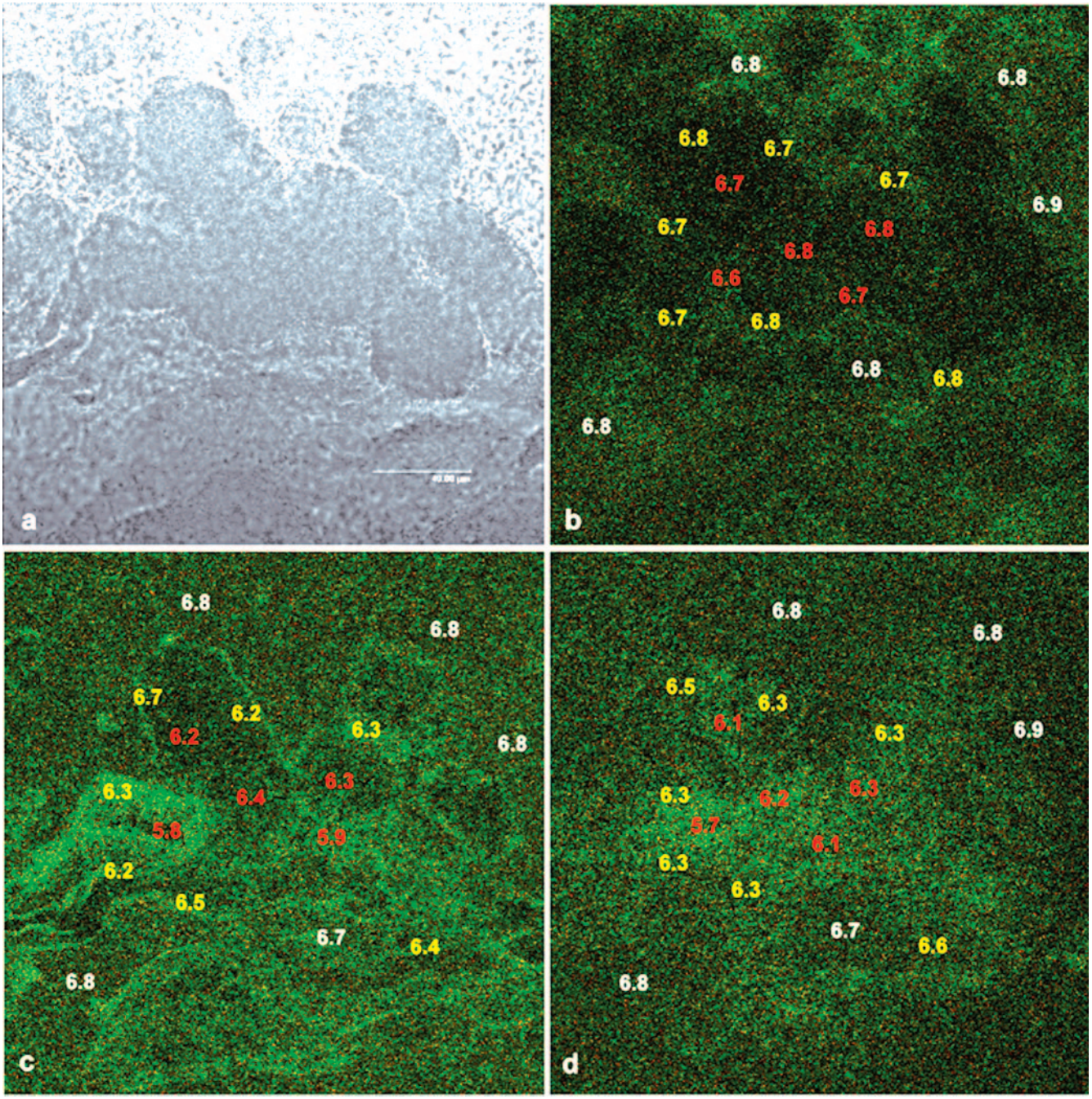

FIG. 5. Bright-field (a) and ratiometric CSLM image slices (b, c, and d) of a C-SNARF-4-treated biofilm at 5 μm (b), 20 μm (c), and 40 μm (d) from the biofilm-bulk fluid interface. Data shown represent average pH levels over an area of 50 μm^2. pH was determined in the bulk fluid (white), the biofilm-fluid interface (yellow), and deep within the biofilm (red). Although fluorescence intensity may appear different in areas of similar pH, the ratio of red/green intensity is constant, giving a quantitative measure of pH. Frequently, pH values are remarkably different in areas located just a few micrometers away from each other, indicating discrete pH microenvironments throughout the biofilm. Bar, 40 μm.

son, other approaches have been highly sought after to define the physicochemical properties of these microenvironments.

In this work, we describe the use of C-SNARF-4, a single-excitation, dual-emission fluorescent pH indicator in probing pH microenvironments that exist within the *P. aeruginosa* PAO1 biofilm matrix. The pH-sensitive chemical structure of the C-SNARF-4 probe is shown in Fig. 7. Above pH 5, it is assumed that the dye exists as a mixture of two forms, the monoanionic (naphthol) and dianionic (naphtholate) states, between which a pH-sensitive equilibrium is established depending on the acidity or alkalinity of the solution (21, 22). In basic aqueous solutions above pH 9, the phenol and carboxylic acid groups of the probe become completely ionized. It is believed that acidification of a solution first protonates the

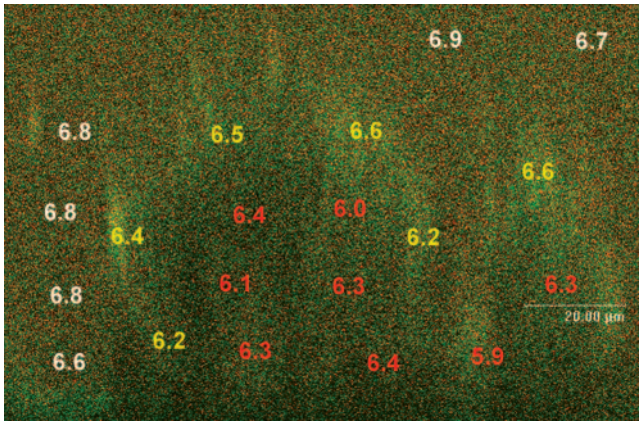

FIG. 6. *x,z* CSLM image section of a C-SNARF-4-treated biofilm. The top represents the biofilm-bulk fluid interface, while the bottom of the image represents the substratum. Average pH values were obtained from 50-μm^2 areas in the bulk fluid (white text), the biofilm-fluid interface (yellow text), and within the microcolony (red text). Bar, 20 μm.

phenol group (pK_a ~6.4) of the dianion to yield the C-SNARF-4 monoanion. Though further acidification below pH 5 generates neutral and cationic forms of the dye, these forms are nonfluorescent and contribute little to the emission properties of the dye molecule (Molecular Probes Technical Support, personal communication). Generation of the naphthol species through acidification alters the emission spectrum of the probe, so that acidic conditions increase the intensity of the probe at 580 nm and decrease it (or keep it constant, depending on instrumentation sensitivity) at 640 nm. As shown here, the ratio between both wavelengths (640 nm/580 nm) is independent of probe concentration, which is consistent with previous studies (34). This allows the relative concentrations of the protonated and unprotonated forms to be quantified, providing an accurate and reliable measure of pH in a given environment. These pH-sensitive properties of C-SNARF probes have been used successfully in quantifying pH in perfused myocardium (34), mitochondria (46), internal pH in *Saccharomyces cerevisiae* (2), and several other eukaryotic systems. To our knowledge, this is the first time that the use of a C-SNARF probe has been applied to the study of biofilms.

The use of C-SNARF probes has several advantages over other available techniques. Most importantly, spectral characteristics of these fluorophores permit dual-emission ratiometric imaging. As a result, fluorescent intensity in a given environment is independent of probe concentration, overcoming theoretical problems due to compartmentalization or sequestration of the probe. Another potential limitation of fluorescent pH imaging is the loss of fluorescence intensity due to the inner filter effect of thick samples. It has previously been shown, however, that SNARF emissions are not affected in semisolid media up to 200 μm in thickness (much thicker than *P. aeruginosa* biofilms) (34). C-SNARF probes have also been found to become photosensitive over lengthy experiments (11), which could be a significant limitation. However, one study suggests that C-SNARF probes are only sensitive to photobleaching above pH 7.3 (i.e., the protonated form), since most light is absorbed by the protonated dye (5). As the pH is increased above the pK_a of the probe, the unprotonated form absorbs the bulk of the incident light, and bleach rates are increased. Since the pK_a of C-SNARF-4 is lower than that of other SNARF probes, it may be sensitive to photobleaching at lower pH levels. However, it has been noted that in short-term experiments such as this one, pH equilibration of the probe occurs much faster than photobleaching, otherwise, emission ratios would be homogeneous throughout the sample.

Although fluorescent imaging with C-SNARF-4 may contribute to our understanding of biofilm physiology, inherent restrictions of the probe may preclude its use in some environments. For example, the pK_a (~6.4) of C-SNARF-4 may limit its use in some acidophilic biofilms such as dental biofilms, where pH levels have been shown to drop down below pH 3 following fermentation of dietary carbohydrates (50). Photon absorption and scatter may also restrict their use in thick biofilms or deep microbial mats, which often exceed 10 cm in thickness. Microelectrodes remain a more attractive option in these applications. Another minor drawback of C-SNARF

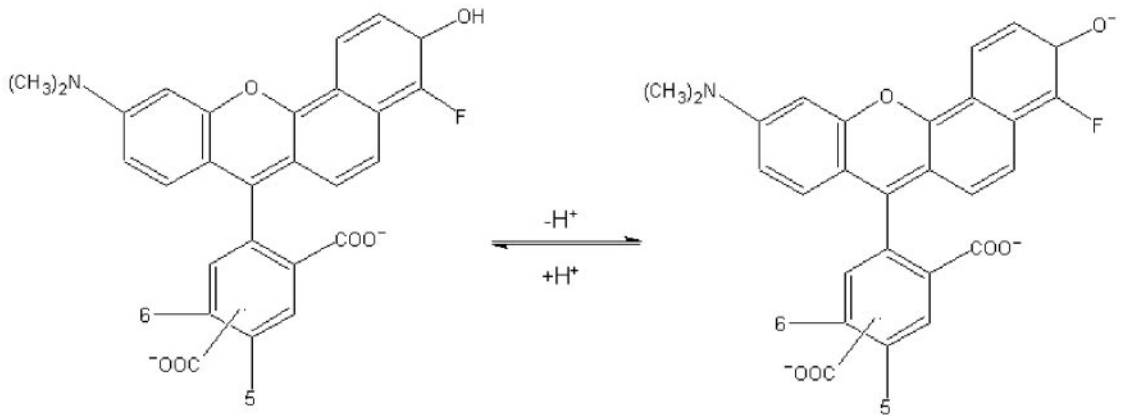

FIG. 7. Chemical structure and pH-dependent equilibrium of C-SNARF-4. As pH is lowered, protonation of the phenol group (pK_a = 6.4) of the monoanion (naphthol form) yields the dianion (naphtholate form). The concentration of each is determined by the acidity or alkalinity of the microenvironment. Since each form has a characteristic emission maximum at different wavelengths (580 nm and 640 nm), fluorescence emission ratios can reliably be used to quantitatively determine pH.

probes would be when the pH of the system is near that of the surrounding milieu (46). Here, pH-dependent emission intensity may make it difficult to distinguish boundary layers of the biofilm (i.e., biofilm-fluid interface), requiring localization information to be obtained at the same time (i.e., phase-contrast light microscopy). Finally, even though the spatial organization of pH microenvironments may be such that they approach smaller so-called nanoenvironments or beyond, quantification of pH using these techniques is limited by the resolution of the digital image. As can be expected, detector resolution of the confocal microscope surpasses what can be represented in a micrograph.

Interactions of fluorescent probes with matrix components could also potentially complicate usage of any indicator. For example, Večeř et al. (48), House (23), and Seksek et al. (42) have all described non-pH related interactions of SNARF probes with eukaryotic intracellular compounds, presumably by charge-charge interaction. Our study, however, shows that the interaction of C-SNARF-4 with alginic acid, BSA, or growth medium at natural pH and below does not seem to influence fluorescence emission characteristics of the probe. Alginic acid (alginate), a heteropolymer of mannuronic and guluronic acids, is often suggested to be the dominant extracellular polymeric substance component in mucoid *P. aeruginosa* biofilms. It should be noted, however, that this polymer is not normally produced by common laboratory strains such as PAO1 (43, 53). Yet, highly charged polymers such as alginate are frequently encountered in natural biofilms of all sorts. For this reason, we feel that alginate provides a suitable control polymer due to its highly anionic nature, while providing a convenient model compound to mimic interactions between C-SNARF-4 and microbial polymers. Interestingly, no deleterious interactions were observed between alginate and C-SNARF-4 at pH 7.0 or below. Only at pH 7.2 and above did emission ratios slightly change. Though BSA is not a component of biofilm matrices, it provides a well-characterized model macromolecule to assess interactions of C-SNARF-4 with biofilm matrix proteins. BSA contains a high content of charged amino acids (Asp, Gln, Lys, and Arg) and cystine residues, is able to reversibly bind a wide variety of ligands, and undergoes conformational isomerization with changes in pH (26), making this protein a likely candidate to influence the fluorescence properties of C-SNARF-4. Surprisingly, at neutral pH and below, no change in ratio was observed when C-SNARF-4 was incubated with various concentrations of BSA. These results differ from those previously reported (42), which show a significant alteration in emission spectra. More recently, however, it was determined that the SNARF variant used in that study (C-SNARF-1) contained a contaminant able to bind to BSA, which led to discrepancies between intracellular and cell-free spectral properties (55). C-SNARF-4 differs from the probe used in that study as it has a lower pKa value (6.4 compared to 7.5) due to a fluorine atom, and it lacks the acetoxymethylester substituent. These may contribute to different interactions with BSA. Lipid-associated molecules (i.e., lipoproteins) and nucleic acids are also known to be common components of biofilm matrices, although they were not investigated in this study. It has been established, however, that lipids (42, 48) and double-stranded and heat-denatured DNA (42) induce no change in SNARF-1 fluorescence.

When C-SNARF-4 was incubated with alginate and BSA above pH 7, it showed a concentration dependent change in ratio, which translated into a pH difference of 0.2 to 0.3 units. It is likely that at higher concentrations of alginate and BSA there would be even greater discrepancies. However, EPS frequently exists at a concentration of 1 to 2% (wt/vol) in natural biofilms (18, 19). It is possible that some microenvironments may be less hydrated and contain a higher concentration of EPSs, but in our opinion, under most circumstances, natural EPS and protein (and presumably other exopolymer) concentrations should not be a hindrance with C-SNARF-4 ratiometric staining. Yet, alkaline systems may generate significant errors in pH measurements when this probe is used to determine microenvironment pH. This would be especially true if there is a heterogeneous distribution of EPS throughout the matrix.

The principal findings of this research demonstrate that CSNARF-4 can be used as a reliable quantitative indicator of pH in microenvironments of *P. aeruginosa* biofilms in situ. At low matrix densities, there is so little interaction between probe and exopolymer that emission spectra are not altered. With a calibration curve obtained in cell-free pH-adjusted buffer solutions and once fluorescence ratios in C-SNARF-4-treated biofilms were converted to $[H^+]$, this probe revealed significant pH heterogeneity in microenvironments at all x, y, and z zones of the biofilm matrix, suggesting diverse microbial metabolic rates and restricted diffusion of nutrients, wastes, and other acidic metabolites throughout the biofilm.

The spatial variation in pH shown in this study may have several implications for biofilm structure and function. For example, Stoodley et al. (44) revealed that changes in bulk fluid pH alter the physical properties of a biofilm, reducing the thickness of a biofilm by 30% when grown in pH 3 buffer, relative to those grown at neutral pH. This is to be expected with matrix biopolymers that are ionizable and depend on electrostatic interaction. pH should contribute to most physicochemical properties such as polymer-polymer, ion-polymer, and macromolecule-polymer interactions, and even polymer motion, gyration, and polymer-polymer entwining. From a clinical perspective, a pH gradient that ranges from 5.6 to 7.0 could potentially alter such rheological properties so that the biofilm matrix could serve as a significant physical barrier to antibiotic penetration through size-dependent exclusion of molecules from the EPS matrix (29). A change in matrix chemistry (as a result of pH) may also lead to protonation-deprotonation of an incoming antibiotic such that matrix polymers inhibit the action of these biocides through sorption and/or inactivation.

Biofilm biogeochemistry is also highly sensitive to changes in pH. For example, Barker et al. (4) have identified a strong dependence of mineral dissolution and bioweathering rates on pH, which are likely affected by pH microenvironments. Ferris et al. (17) also showed that metal uptake by wastewater biofilms was 12-fold greater at pH 7.0 than at pH 3.1. Since biofilms have been explored in potential bioremediative applications, understanding the effect of microenvironments on biofilm-metal uptake processes is highly desirable, so as to manipulate these systems to our advantage. Other previous studies (8, 9, 27, 28, 30) have proposed that pH and redox fluctuations in microenvironments could cause a heterogeneous distribution of mineral phases within natural biofilms.

On a geological time scale, it is believed that by locally mediating solution chemistry, subpopulations of microbes within a biofilm can ultimately determine the state and availability of a metal, so that different mineral phases that form only under discrete geochemical conditions (pH and E_h; e.g., goethite, hematite, and magnetite) form within micrometers of one another. The pH distribution in our study (pH 5.6 to pH 7.0) may not be sufficient to explain mineral distributions described in previous studies; however, iron Pourbaix diagrams suggest that if the differential diffusion or metabolism of oxygen generates regions of low E_h, pH gradients observed in this study may indeed create localized geochemistry that promotes the formation of discrete mineral phases. The spatial distribution of these mineral precipitates may serve as a micrometer-scale analogue to larger sedimentary deposits such as banded iron formations (10).

Our present study should help in the understanding of the role pH in microenvironments plays in the medical and geobiological role of natural biofilms. We are currently exploring the geobiological aspects.

ACKNOWLEDGMENTS

R.C.H. was funded through a Natural Science and Engineering Council of Canada (NSERC) graduate fellowship, and the experimentation was funded through NSERC—Discovery and Advanced Food and Materials Network (AFMnet)-National Centres of Excellence grants to T.J.B.

REFERENCES

1. **Allan, V. J. M., L. E. Macaskie, and M. E. Callow.** 1999. Development of a pH gradient within a biofilm is dependent upon the limiting nutrient. Biotechnol. Lett. **21:**407–413.
2. **Aon, J. C., and S. Cortassa.** 1997. Fluorescent measurement of the intracellular pH during sporulation of *Saccharomyces cerevisiae*. FEMS Microbiol. Lett. **153:**17–23.
3. **Ariyoshi, H., and E. W. Salzman.** 1995. Spatial distribution and temporal change in cytosolic pH and [Ca^2+] in resting and activated single human platelets. Cell Calcium **17:**317–326.
4. **Barker, W. W., S. A. Welch, S. Chu, and J. F. Banfield.** 1998. Experimental observations of the effects of bacteria on aluminiosilicate weathering. Am. Mineral. **83:**1551–1563.
5. **Bassnett, S., L. Reinsch, and D. C. Beebe.** 1990. Intracellular pH measurement using single excitation-dual emission fluorescence ratios. Am. J. Physiol. **258:**C171–C178.
6. **Beyenal, H., and Z. Lewandowski.** 2000. Combined effect of substrate concentration and flow velocity on effective diffusivity in biofilms. Water Res. **34:**528–538.
7. **Blank, P. S., H. S. Silverman, O. Y. Chung, B. A Hogue, M. D. Stern, R. G. Hansford, E. G. Lakatta, and M. C. Capogrossi.** 1992. Cytosolic pH measurements in single cardiac myocytese using carboxy-seminaphthorhodafluor-1. Am. J. Physiol. **263:**H276–H284.
8. **Brown, D. A., T. J. Beveridge, C. W. Keevil, and B. L. Sheriff.** 1998. Evaluation of microscopic techniques to observe iron precipitation in a natural biofilm. FEMS Microbiol. Ecol. **26:**297–310.
9. **Brown, D. A., D. C. Kamineni, J. A. Sawicki, and T. J. Beveridge.** 1994. Minerals associated with biofilm occurring on exposed rock in a granitic underground research laboratory. Appl. Environ. Microbiol. **60:**3182–3191.
10. **Brown, D. A., J. A. Sawicki, and B. L. Sheriff.** 1998. Alteration of microbially precipitated iron oxides and hydroxides. Am. Mineral. **83:**1419–1425.
11. **Buckler, K. J., and R. D. Vaughn-Jones.** 1990. Application of a new pH-sensitive fluoroprobe (carboxy-SNARF-1) for intracellular pH measurement in small isolated cells. Pflugers Arch. **417:**234–239.
12. **Caldwell, D. E., D. R. Korber, and J. R. Lawrence.** 1992. Confocal laser microscopy and digital image analysis in microbial ecology. Adv. Microbiol. Ecol. **12:**1–67.
13. **Cormack, B. P., R. H. Valdivia, and S. F. Falkow.** 1996. FACS-optimized mutants of the green fluorescent protein. Gene **173:**33–38.
14. **Costerton, J. W., Z. Lewandowski, D. DeBeer, D. Caldwell, D. Korber, and G. James.** 1994. Biofilms, the customized microniche. J. Bacteriol. **176:**2137–2142.
15. **De Beer, D., R. Srinivasan, and P. S. Stewart.** 1994. Direct measurement of chlorine penetration into biofilms during disinfection. Appl. Environ. Microbiol. **60:**4339–4344.
16. **de los Rios, A., J. Wierzchos, L. G. Sancho, and C. Ascaso.** 2003. Acid microenvironments in microbial biofilms of Antarctic endolithic microecosystems. Environ. Microbiol. **5:**231–237.
17. **Ferris, F. G., S. Schultz, T. C. Witten, F. C. Fyfe, and T. J. Beveridge.** 1989. Metal interactions with microbial biofilms in acidic and neutral pH environments. Appl. Environ. Microbiol. **55:**1249–1257.
18. **Flemming, H. C., and J. Windenger.** 2001. Relevance of microbial extracellular polymeric substances (EPSs)—part I: structural and ecological aspects. Water Sci. Technol. **43:**1–8.
19. **Flemming, H. C., J. Windenger, C. Mayer, V. Korstgens, and W. Borchard.** 2000. Cohesiveness in biofilm matrix polymers, p. 87–105. *In* D. G. Allison, P. Gilbert, H. M. Lappin-Scott, and M. Wilson (ed.), Community structure and co-operation in biofilms, SGM symposium series vol. 59. Cambridge University Press, Cambridge, United Kingdom.
20. **Gordon, C. A., N. A. Hodges, and C. Marriott.** 1988. Antibiotic interaction and diffusion through alginate and exopolysaccharide of cystic-fibrosis-derived *Pseudomonas aeruginosa*. J. Antimicrob. Chemother. **42:**974–977.
21. **Haugland, R. P.** 1992. Handbook of fluorescent probes and research chemicals, 6th ed. Molecular Probes, Eugene, Oreg.
22. **Haugland, R. P, and J. Whitaker.** July 1990. Xanthene dyes having a fused (C) benzo ring. U.S. patent 4,945,171.
23. **House, C. R.** 1994. Confocal ratio-imaging of intracellular pH in unfertilized mouse oocytes. Zygote **2:**37–45.
24. **Hoyle, B. D., and J. W. Costerton.** 1991. Bacterial resistance to antibiotics. The role of biofilms. Prog. Drug. Res. **37:**91–105.
25. **Hoyle, B. D., C. K. W. Wong, and J. W. Costerton.** 1992. Disparate efficacy of tobramycin on Ca^{2+}-, Mg^{2+}-, and HEPES-treated *Pseudomonas aeruginosa* biofilms. Can. J. Microbiol. **38:**1214–1218.
26. **Jones, T., Jr.** 1996. All about albumin: biochemistry, genetics, and medical applications. Academic Press, Inc., Orlando, Fla.
27. **Karthhikeyan, S., and T. J. Beveridge.** 2002. *Pseudomonas aeruginosa* biofilms react with and precipitate toxic soluble gold. Environ. Microbiol. **4:**667–675.
28. **Langley, S., and T. J. Beveridge.** 1999. Metal binding by *Pseudomonas aeruginosa* PAO1 is influenced by growth of the cells as a biofilm. Can. J. Microbiol. **45:**616–622.
29. **Lawrence, J. R., G. M. Wolfaardt, and D. R. Korber.** 1994. Monitoring diffusion in biofilm matrices using confocal laser microscopy. Appl. Environ. Microbiol. **60:**1166–1173.
30. **Lee, J.-U., and T. J. Beveridge.** 2001. Interaction between iron and *Pseudomonas aeruginosa* biofilms attached to Sepharose surfaces. Chem. Geol. **180:**67–80.
31. **Lewis, K.** 2001. Riddle of biofilm resistance. Antimicrob. Agents Chemother. **45:**999–1007.
32. **Liehr, S. K.** 1995. Effect of pH on metals precipitation in denitrifying biofilms. Water Sci. Technol. **32:**179–183.
33. **Martinez-Zaguilan, R., M. W. Gurule, and R. M. Lynch.** 1996. Simultaneous measurement of intracellular pH and Ca^{2+} in insulin-secreting cells by spectral imaging microscopy. Am. J. Physiol. **270:**C1438–C1446.
34. **Muller-Borer, B. J., H. Yang, S. A. Marzouk, J. J. Lemasters, and W. E. Cascio.** 1998. pH_i and pH_o at different depths in perfused myocardium measured by confocal fluorescence microscopy. Am. J. Physiol. **275:**H1937–H1947.
35. **Nichols, W. W., S. M. Dorrington, M. P. E. Slack, and H. L. Walmsley.** 1988. Inhibition of tobramycin diffusion by binding to alginate. Antimicrob. Agents Chemother. **32:**518–523.
36. **Nivens, D. E., D. E. Ohman, J. Williams, and M. J. Franklin.** 2001. Role of alginate and its O acetylation in formation of *Pseudomonas aeruginosa* microcolonies and biofilms. J. Bacteriol. **183:**1047–1057.
37. **Okabe, S., T. Kindaichi, T. Ito, and H. Satoh.** 2004. Analysis of size distribution and areal cell density of ammonia-oxidizing bacterial microcolonies in relation to substrate microprofiles in biofilms. Biotechnol. Bioeng. **85:**86–95.
38. **Owen, C. S.** 1992. Comparison of spectrum-shifting intracellular pH probes 5′(and 6′)-carboxy-10-dimthylamino-3-hydroxyspiro[7H-benzo-[c]xanthene-7,1′(3′H)-isobenzofuran]-3′-one and 2′,7′-biscarboxy-ethyl-5(and 6)-carboxyfluorescein. Anal. Biochem. **204:**65–71.
39. **Ramsing, N. B. M. Kühl, and B. B. Jørgensen.** 1993. Distribution of sulfate-reducing bacteria, O_2, and H_2S in photosynthetic biofilms determined by oligonucleotide probes and microelectrodes. Appl. Environ. Microbiol. **59:**3840–3849.
40. **Sanders, R., A. Draaijer, H. C. Gerritsen, P. M. Houpt, and Y. K. Levine.** 1995. Quantitative pH imaging in cells using confocal fluorescence lifetime imaging microscopy. Anal. Biochem. **227:**302–308.
41. **Schramm, A., L. H. Larsen, N. P. Revsbech, N. B. Ramsing, R. Amann, and K. H. Schleifer.** 1996. Structure and function of a nitrifying as determined by in situ hybridization and the use of microelectrodes. Appl. Environ. Microbiol. **62:**4641–4647.
42. **Seksek, O., N. Henry-Toulme, F. Sureau, and J. Bolard.** 1991. SNARF-1 as an intracellular pH indicator in laser microspectrofluorometry: a critical assessment. Anal. Biochem. **193:**49–54.
43. **Stapper, A. P., G. Narasimhan, D. E. Ohman, J. Barakat, M. Hentzer, S. Molin, A. Kharazmi, N. Hoiby, and K. Mathee.** 2004. Alginate production

affect *Pseudomonas aeruginosa* biofilm development and architecture, but is not essential for biofilm development. J. Med. Microbiol. **53:**679–690.
44. **Stoodley, P., D. de Beer, and H. M. Lappin-Scott.** 1997. Influence of electric fields and pH on biofilm structure as related to the bioelectric effect. Antimicrob. Agents Chemother. **41:**1876–1879.
45. **Szmacinski, H., and J. R. Lakowicz.** 1993. Optical measurements of pH using fluorescent lifetimes and phase modulation fluorometry. Anal. Chem. **65:** 1668–1674.
46. **Takahashi, A., Y. Zhang, E. Centonze, and B. Herman.** 2001. Measurement of mitochondrial pH in situ. BioTechniques **30:**804–808.
47. **Tsien, R. Y., and M. Poenie.** 1986. Fluorescence ratio imaging: a new window into intracellular ionic signaling. Trends Biochem. Sci. **11:**450–455.
48. **Večeř, J., A. Holoubek, and K. Sigler.** 2001. Fluorescence behavior of the pH-sensitive probe carboxy SNARF-1 in suspension of liposomes. Photochem. Photobiol. **74:**8–13.
49. **Villaverde, S., R. G. Mirpuri, Z. Lewandowski, and W. L. Jones.** 1997. Physiological and chemical gradients in a *Pseudomonas putida* 54G biofilm degrading toluene in a flat plate vapor phase bioreactor. Biotechnol. Bioeng. **56:**361–371.
50. **Vroom, J. M., K. J. de Grauw, H. C. Gerritsen, D. J. Bradshaw, P. D. Marsh, G. K. Watson, J. J. Birmingham, and C. Allison.** 1999. Depth penetration and detection of pH gradients in biofilms by two-photon excitation microscopy. Appl. Environ. Microbiol. **65:**3502–3511.
51. **Walters, M. C., III, F. Roe, A. Bugnicourt, M. J. Franklin, and P. S. Stewart.** 2003. Contributions of antibiotic penetration, oxygen limitation, and low metabolic activity to tolerance of *Pseudomonas aeruginosa* biofilms to ciprofloxacin and tobramycin. Antimicrob. Agents Chemother. **47:**317–323.
52. **Westerblad, H., J. D. Bruton, and J. Lannergren.** 1997. The effect of intracellular pH on contractile function of intact, single fibres of mouse muscle declines with increasing temperature. J. Physiol. **500:**193–204.
53. **Wozniak, D. J., T. J. O. Wyckoff, M. Starkey, R. Keyer, P. Azadi, G. A. O'Toole, and M. R. Parsek.** 2003. Alginate is not a significant component of the extracellular polysaccharide matrix of PA14 and PAO1 *Pseudomonas aeruginosa* biofilms. Proc. Natl. Acad. Sci. USA **100:**7907–7912.
54. **Xu, K. D., P. S. Stewart, F. Xia, C. T. Huang, and G. A. McFeters.** 1998. Spatial physiological heterogeneity in *Pseudomonas aeruginosa* biofilm is determined by oxygen availability. Appl. Environ. Microbiol. **64:**4035–4039.
55. **Yassine, M., J. M. Salmon, J. Vigo, and P. Viallet.** 1995. C-SNARF-1 as a pH_i fluoroprobe: discrepancies between conventional and intracellular data do not result from protein interactions. J. Photochem. Photobiol. B, Biol. **37:**18–25.
56. **Yu, T., and P. L. Bishop.** 2001. Stratification and oxidation-reduction potential change in an aerobic and sulfate-reducing biofilm studied using microelectrodes. Water Environ. Res. **73:**368–373.